Title

Histone variant H3.3 mediates cGAS-STING pathway activation via telomere deprotection

Authors and affiliations

Chiao-Ming Huang and Liuh-Yow Chen

Molecular and Cell Biology, Taiwan International Graduate Program, Academia Sinica and Graduate Institute of Life Science, National Defense Medical Center, Taipei City 11490, Taiwan

Abstract

Telomeric deposition of histone variant H3.3 is controlled by ATRX, DAXX, HIRA, and ASF1 proteins. Point mutations of H3.3 and defective mutants of ATRX are associated with cancers that utilize the alternative lengthening of telomeres (ALT) pathway to protect and maintain chromosome ends. Here, we identify a cascade of events following the expression of a TRF2 dominant negative mutant, TRF2ΔBΔM, which are regulated by H3.3 expression. H3.3 regulates the formation of damaged foci at telomeres and subsequent telomere-to-telomere fusion events controlled by the DNA repair pathway. Telomere fusion events also contributes to the formation of micronuclei and abnormal segregation. Micronuclei formation triggers activation of the cGAS-STING mediated innate immune response to intracellular DNA and inhibits cell growth. All of these phenotypes are controlled by the expression of H3.3. Additionally, disruption of ATRX, DAXX, HIRA, or ASF1 elicits an impairment phenotype similar to that is caused by H3.3 inhibition. Our results indicate that cGAS-STING-mediated cellular senescence is triggered by deprotected telomeres and is controlled by the expression and deposition of H3.3 on telomeres.

Introduction

Protection of chromosome ends is the crucial function of telomeres and telomere-associated proteins. Disruption of telomere protection leads to replicative senescence (1-3). Shelterin protein Telomeric Repeat binding Factor 2 (TERF2, TRF2) plays a central role in protecting telomeres from damage response. Expression of dominant-negative TRF2 leads to cellular senescence that accompany with the formation of fused chromosome ends, which comes from joining of telomeric sequence (2). Furthermore, expressing dominant-negative TRF2 in ataxia-telangiectasia patient-derived culture cells impairs the activation of p53 response (4). The observation indicates that lake of TRF2 contributes to activation of an Ataxia Telangiectasia Mutated (ATM)-mediated DNA damage response (2-4). Similarly, double strand break (DSB) repair machinery sensed by Meiotic Recombination 11 (MRE11)- RAD50 Double Strand Break Repair Protein (RAD50)- Nibrin (NBN, NBS1) (MRN) complex and activated ATM to facilitate p53-dependent checkpoint response, including senescence (5-7). Additionally, the repair mechanism molecules that downstream of ATM activation are responsible for TRF2-associated telomere fusion. Those molecules include Ku protein 70/80, Ligase IV (LIG4), and X-ray Repair Cross Complementing 4 (XRCC4) (2,8,9). Those observations indicated a well-established mechanism that deprotection of telomere by manipulating TRF2 contributes to a ATM-dependent checkpoint response, and this response further mediated by DSB repair machinery and drives to senescence.

Recently, telomere dysfunction has been linked to activation of the intracellular DNA sensing pathway mediated by Cyclic GMP-AMP Synthase (cGAS) (10). The cGAS-STING pathway were known as an innate immune pathway for sensing cytosolic DNA, and triggers type-I interferon response (11). In the cGAS-STING pathway, cytosolic double strand DNA is sensed by cGAS, which synthesizes cyclic GMP-AMP (cGAMP) as a second messenger. cGAMP can sensed by endoplasmic reticulum (ER)-bound Stimulator of interferon response cGAMP interactor (STING), and drives the following response, including the Interferon regulatory factor 3 (IRF3)-dependent type-I interferon production (11,12). Besides the direct association between cGAS pathway and telomere dysfunction, the indirect evidences were also observed. For example, the chromatin bridges induced by dominant-negative mutant of TRF2 were found to be processed by the enzyme Three Prime Repair Exonuclease 1 (TREX1) (13). DNA fragments degraded by TREX1 activate the cGAS-STING response (14). Additionally, a TRF2 mutant, TRF2ΔB, is observed that triggers formation of extrachromosomal telomere repeats (ECTRs), driving activation of the cGAS-STING response (15). These direct and indirect lines of evidence imply that the phenotypes caused by deprotected telomeres are associated with activation of the cGAS-STING signaling pathway, potentially via expression of cytokines such as interferons (IFNs) and interleukins (ILs).

The histone variant H3.3 (denoted H3.3) displays a unique regulatory mechanism. It can be deposited by the Histone Cell Cycle Regulator (HIRA) complex on euchromatin, and by the Alpha-Thalassemia/mental Retardation syndrome X-linked (ATRX)-Death domain associated protein (DAXX) complex on heterochromatin, centromeres and telomeres, in a replication-independent manner (16). Although H3.3 deposition is linked to the expression of active genes (17-21), studies exploring the roles of H3.3 on telomeres have been limited. Nevertheless, it has been reported that H3.3 on telomeres in stem cells is phosphorylated at residue S31 (22). Moreover, the ATRX-DAXX complex was found to deposit H3.3 at telomeres

in mouse embryonic stem cells (mESCs) (23) and mouse embryonic fibroblasts (MEFs) (24). Notably, dysregulated deposition and expression of H3.3 mutants have been associated with cancers utilizing the alterative lengthening of telomeres (ALT) pathway (25-28). These observations imply that an ATRX-DAXX-dependent deposition of H3.3 on telomeres and $H3.3^{S31}$ phosphorylation contributes to the formation of ALT cancers.

Here, we report a role for H3.3 on telomeres in the DNA damage response, as well as repair of deprotected telomeres. These responses further contribute to the activation of the cGAS-STING-mediated innate immune response and growth inhibition.

Material and Methods

Cell lines

Cell lines were obtained from ATCC and maintained under their recommended culturing conditions. BJ^t cells originated from BJ normal fibroblasts that stably express hTERT. Retroviral transformation was performed to generate cells that inducibly express green fluorescence protein (GFP), the TRF2 mutant TRF2ΔBΔM, or the TPP1 mutant TPP1ΔRD. Cells were tested for target protein expression by treating with a minimum of 25 ng/ml of doxycycline.

Gene silencing

The siRNAs used were On-target plus siRNA reagents (Dharmacon). The siRNA reagents were generated using the SMARTselection algorithm, with chemical modifications to eliminate off-target effects. Four siRNAs for each of H3F3A, H3F3B, cGAS, LIG4, XRCC4, ATRX, DAXX, HIRA, ASF1A, and ASF1B, as well as two siRNAs for NBS1, were employed. siRNAs were transfected into the cells using Lipofectamine RNAiMAX (Invitrogen) according to the manufacturer's instructions. Depletion of H3.3 and ASF1 was performed by mixing equal amounts of siRNAs targeting H3.3 and ASF1.

Protein extraction, Western blots and antibodies

Cell extracts were harvested using 1 X SDS sample buffer (62.5 mM Tris, pH 6.8, 10% glycerol, 2% SDS, 0.01% bromophenol blue, and 10% β-mercaptoethanol). Proteins were denatured by heating the extract at 95 ^{o}C for 10 minutes. Proteins were separated by SDS-PAGE, and transferred to a nitrocellulose membrane. The membranes were blocked with either Tris-buffered saline at pH 8.0 with 5% milk and 0.1% Tween-20 to determine phosphorylated proteins or using Phosphate-buffered saline at pH 8.0 with 5% milk and 0.1% Tween-20 to determine other proteins. Primary antibodies including phosphorylated STING (19781, Cell Signaling), STING (MAB7169, R&D Systems), cGAS (15102, Abcam), H3.3 (09-838, Merkmillpore; ab176840, Abcam), myc (SI-M4439, Sigma), LIG4 (12695-1-AP, Proteintech), XRCC4 (15817-1-AP, Proteintech), ATRX (A301-045A, Bethyl), DAXX (A301-353A, Bethyl), HIRA (04-1488, Sigma-Aldrich), and ASF1 (sc-53171, Santa Cruz Biotechnology) were used at 1:1000 dilution. Horseradish peroxidase-conjugated secondary antibodies were used at 1:2000 dilution to determine the proteins in samples. As an internal control for gene expression, HRP-conjugated GAPDH antibody (HRP60004, ProteinTech) and HRP-labeled ACTB (HRP-60008, ProteinTech) were used at 1:5000 dilution. Either enhanced chemiluminescence (ECL) or SuperSignal West Femto Maximum Sensitivity reagents (Thermo Fisher Scientific) were used for signal detection.

RNA extraction and quantitative real-time PCR

Cells were lysed and harvested to extract total RNA using an RNA Mini Kit (Amersham). Reverse transcription was performed with iScript Reverse Transcriptase Supermix (Bio-Rad) to generate cDNA for quantitative analyses. Quantitative real-time PCR was performed using SYBR Green Select reagent (LifeTechnologies) to determine expression levels of target genes. Quantitative PCR analysis was performed using a QuantStudio 12K Flex Real-Time PCR System

(ThermoFisher Scientific). The primer sequences are as follows: β-actin, 5'-AGCACTGTGTTGGCGTACAG-3' and 5'-TCCCTGGAGAAGAGCTACGA-3'; interferon β, 5'-AAACTCATGAGCAGTCTGCA-3' and 5'-AGGAGATCTTCAGTTTCGGAGG-3'. Data analysis was performed by calculating the comparative Ct (ΔΔCt) of target genes normalized to an internal control (β-actin).

Metaphase spread and telomere FISH on chromosomes

Analysis of telomere-to-telomere fusion was performed in DOX-treated cells subjected to siRNA-mediated gene expression depletion. Cells were treated with DOX for 30 h, and reseeded in 0.1 μg/ml Demecolcine-containing medium. After 18 h of incubation, the floating and attached cells were collected for further analysis. Cells were incubated with 75 mM KCl for 15 mins at 37 ^{o}C and routinely mixed at 5-minute intervals. Following KCl incubation, the cells were fixed with fix buffer (3:1 methanol:acetic acid) at 4 ^{o}C for more than 24 h. Fixed cells were dropped on a glass slide from a height of 20 cm, heated at 75 ^{o}C for 1 min, and then dried at room temperature overnight. The slides were stained according to a standard fluorescence in situ hybridization (FISH) FISH protocol. In brief, the slides were fixed with 10% formalin for 2 mins, and then dehydrated by incubating them in increasing percentages of ethanol solution. The slides were dried and incubated with a probe mixture (70% formamide, 0.5% blocking reagent (Roche), 250 nM TMR-conjugated $(CCCTAA)_3$-PNA probe, 10 mM Tris pH 7.4) at 80 ^{o}C for 3 mins. The slides were hybridized at room temperature in the dark for 3 h. Serial wash steps were then performed, including twice with Wash I (70% formamide, 10 mM Tris-HCl pH 7.5), and twice with Wash II (100 mM Tris-HCl pH 7.5, 150 mM NaCl, 0.08% Tween-20). The slides were counterstained with DAPI, dehydrated with ethanol, and mounted with Fluoromount Aqueous Mounting Medium (Sigma). Images were acquired with a Zeiss Axio Imager Z1 System. Determination and quantitative analysis of telomere fusion events were performed manually by counting for 700 to 1500 chromosome pairs.

Immunofluorescence staining

Cells grown on coverslips were treated with permeabilization solution (20 mM Hepes pH 8.0, 50 mM NaCl, 3 mM $MgCl_2$, 0.5% Triton-X 100, 300 mM sucrose), and fixed with 2% paraformaldehyde. The cells were permeabilized with 0.5% Triton-X 100, and then blocked with 2% fetal bovine serum (FBS) in phosphate-buffered saline. Primary antibodies including anti-TRF1 (90549, GeneTex) and anti-γH2AX (05-636, Millipore) were used. The secondary antibodies were Mouse IgG Alexa Fluor 488 (A-11001, Invitrogen) and Rabbit IgG Alexa Fluor 555 (A32727, Invitrogen). The cells were stained with DAPI, dehydrated and mounted with ProLong Gold Antifade Mountant (Life Technologies). Images were acquired under a DeltaVision Deconvolution Microscope. Colocalization events were determined based on overlapping of signals from different channels, and quantification was performed by manually counting for > 100 nuclei on one coverslip.

Chromatin immunoprecipitation (ChIP)

The chromatin immunoprecipitation protocol were adapted from Abcam ChIP kit (Ab500). After depletion of gene expression by siRNAs for 4 days, the BJ^t cells were fixed with 1% formaldehyde for 10 min. The crosslinking process were quenched with glycine, and the cells

were collected from culture dish. Chromatin DNA were extracted from cells, and sheared into 200-500 bp. Sheared chromatin DNAs were immunoprecipitated with antibodies, including H3.3 (09-838, Merkmillpore) and TRF2 (90550, GeneTex) antibodies. Antibody precipitated chromatin DNAs were enriched with protein A beads. The enriched chromatin DNAs were reversed crosslink with proteins and extracted from precipitated DNA pellet. Precipitated DNAs were then loaded on Hybond-XL membrane. The telomeric DNA from each sample were determined with α-P^{32}-dCTP-labelled telomere probe.

Cell growth and quantification of nuclear abnormalities

Cell growth was determined by counting cells in the multi-well culture plates. Cells were plated in 12-well plates and fixed by 2% paraformaldehyde on the fourth day post treatment. The cells were stained with DAPI and imaged using an ImageXpress Micro XLS System (Molecular Devices). For each well, images in 64 fixed regions were taken to quantify numbers of cells inside the well. These images were used to quantify nuclear abnormalities, including nucleoplasmic bridges, nuclear buds, and micronuclei. Such abnormalities were identified based on disformed nuclear structure, and the quantification was performed by manually counting for >2000 nuclei in one sample.

Results

TRF2ΔBΔM expression drives cGAS-mediated growth inhibition

To investigate the signaling pathway induced by the telomeric damage response, we developed an inducible expression system to express TRF2ΔBΔM and TPP1ΔRD in telomerase immortalized BJ human fibroblast (BJ^t) under control by tetracycline-dependent promoter. TRF2ΔBΔM, a deletion mutant of TRF2 lacking its N-terminal basic domain and C-terminal DNA binding domain, suppresses the formation of a functional telomere shelterin complex with endogenous TRF2 and induces telomere uncapping and telomere-to-telomere fusion (2). On the other hand, TPP1ΔRD, the deletion mutant of TPP1 (also known as ACD shelterin complex subunit and telomerase recruitment factor, ACD) lacking the binding domain with Protection of telomeres 1 (POT1), was known for dirving massive telomeric damage in MEF cells (29). Upon adding doxycycline (DOX) to culture medium, TRF2ΔBΔM and TPP1ΔRD were expressed to elicit telomere dysfunction induced foci (TIFs), characterized by telomere localization of DNA damage marker γH2AX (Fig. 3). Intriguingly, a significant increase of phosphorylated STING was detected following DOX-induced expression of TRF2ΔBΔM and TPP1ΔRD, but not GFP (Fig. S1). The association between TRF2ΔBΔM expression and STING phosphorylation was then further characterized. Levels of STING phosphorylation occurred on day 2 and peaked on day 3 post DOX treatment, coinciding with the induction of TRF2ΔBΔM expression (Fig. S2A). Furthermore, reverse transcription (RT) real-time PCR analysis revealed an induction of interferon beta (IFNβ) mRNA expression associated with STING phosphorylation (Fig. S2B), suggesting activation of STING triggered downstream signaling to induce transcriptional induction of IFNβ. This result is reminiscent of previous studies suggesting activation of cGAS-STING pathway. To confirm that cGAS-mediated STING activation upon TRF2ΔBΔM expression, cGAS was depleted by siRNAs before DOX addition. Indeed, depletion of cGAS prevented phosphorylation of STING and induction of IFNβ mRNA levels in TRF2ΔBΔM expressing cells (Fig. 1A, B), suggesting that TRF2ΔBΔM expression activates the cGAS-STING signaling cascade to induce expression of type I interferon.

It has been shown that telomere deprotection upon TRF2ΔBΔM expression causes cell growth arrest and senescence (2). Consistently, DOX-induced expression of TRF2ΔBΔM in BJ^t cells also led to significant cell growth retardation (Fig. 1C). We showed previously that cGAS-STING pathway activation induces IFNβ expression and affect cell proliferation (15). Therefore, it is conceivable that the cell growth defects associated with TRF2DBDM expression might be caused by cGAS-STIMG pathway activation. To examine this possibility, BJ^t cells were transfected with cGAS siRNAs and subjected to cell growth analysis. The result showed that depletion of cGAS could partially rescue cell proliferation of BJ^t cells expressing TRF2ΔBΔM (Fig. 1D), indicating that the induction the cGAS-STING pathway contributes to TRF2ΔBΔM-mediated cell growth defects. Altogether, these data support a fundamental role of cGAS-STING pathway in mediating the cellular effects due to telomere uncapping.

H3.3 regulates activation of cGAS-mediated growth inhibition

We previously showed that H3.3 and its chaperones ATRX-DAXX complex promote cGAS-STING pathway activation in response to extrachromosomal telomere repeat DNA

accumulation upon TRF2ΔB-induced telomere excision (15). Given that ectopic expression of either TRF2ΔB or TRF2ΔBΔM elicit TRF2 dysfunction, we sought to investigate whether histone H3.3 could be involved in the activation of cGAS-STING pathway driven by TRF2ΔBΔM-induced telomere uncapping. To test this possibility, we used siRNA to deplete histone H3.3 in BJ^t cells and examine TRF2ΔBΔM-induced STING phosphorylation and IFNβ induction. The results showed that histone H3.3 depletion significantly diminished STING phosphorylation and IFNβ in BJ^t cells expressing TRF2ΔBΔM (Fig. 2A, B). In addition, the phenotype of cell proliferation defects associated with TRF2ΔBΔM was alleviated when histone H3.3 expression was silenced by siRNA transfection (Fig. 2C). These observations establish the notion that histone H3.3 mediates the activation of the cGAS-STING pathway and subsequent cell growth effects resulting from telomere uncapping.

Histone H3.3 mediates telomere fusion-driven cGAS-STING pathway activation

Telomere uncapping due to TRF2 deficiency results in telomere fusion via the non-homologous end joining (NHEJ) pathway events (2,9,30), which result in micronuclei generation (10,31) and activation of the cGAS-STING pathway (10). We reasoned that activation of the cGAS-STING pathway upon TRF2ΔBΔM expression might result from telomere fusion. To examine this possibility, siRNAs were used to silenced the expression of Ligase IV/XRCC4 complex, which mediates telomere fusion by NHEJ mechanism. Consistently, depletion of Ligase IV or XRCC4 in BJ^t cells diminished TRF2ΔBΔM-induced telomere-telomere fusion (Fig. 4A, B) and formation of abnormal nuclear structures, including nucleoplasmic bridges, nuclear buds, and micronuclei (Fig. 4C, D). Meanwhile, phosphorylation of STING and IFNβ mRNA induction in BJ^t cells were inhibited when the expression of Ligase IV or XRCC4 was silenced (Fig. 5). These results supported that activation of the cGAS-STING pathway upon TRF2ΔBΔM expression could be attributed to the NHEJ-mediated fusion of the uncapped telomeres.

As shown above, histone H3.3 play a role in the activation of cGAS-STING pathway in BJ^t cells with uncapped telomeres. We reasoned that histone H3.3 might be involved in telomere fusion, thus affecting cGAS-STING pathway activation. To examine this possibility, expression of histone H3.3 was silenced in BJ^t cells for the analysis of telomere fusion and nuclear structural abnormalities following TRF2ΔBΔM induction. The results showed that hitsone H3.3 depletion indeed reduced the number of telomere fusion events, as well as formation of micronuclei, nuclear buds, and nucleoplasmic bridges induced by TRF2ΔBΔM expression (Fig. 4), suggesting that histone H3.3 plays a role in telomere fusion upon telomere uncapping. Additionally, our results revealed that chromosomal and nuclear abnormalities occur before the peak of cGAS-STING response (Fig. S2), indicating that histone H3.3 controls activation of that response by regulating those abnormalities. However, depletion of cGAS did not rescue TRF2ΔBΔM-mediated telomere fusion or nuclear abnormalities, which excluded the possibility that cGAS may be involved in DNA repair at telomeres. In summary, there results suggest that histone H3.3 mediated cGAS-STING activation via regulating the repair of uncapped telomeres by NHEJ.

Histone H3.3 regulate activation of telomere DNA damage response (DDR)

Uncapped telomeres activate DDR, which orchestrates DNA repair by NHEJ (9). Additionally, activation of the cGAS-STING pathway by telomere dysfunction is attributable to an inefficient DNA damage response (10). The observations indicate that telomeric DDR can be the initial event that drives DNA repair and activation of the cGAS-STING pathway. To access the telomeric DDR, the levels of DDR was monitored by recording TIFs in cells. TIFs represent markers of damaged telomeres, which are typically evaluated by immunostaining for γH2AX or 53BP1 on telomeres (32). To address whether histone H3.3 regulates cGAS-STING activation by controlling the telomeric damage response upon telomere uncapping, we investigated TIF formation through analyzing telomeric localization of γH2AX by immunostaining. Cells with >5 TIFs in one nucleus were denoted TIF+ cells, representing those displaying severe telomeric damage. Depletion of histone H3.3, but not cGAS, resulted in fewer TIFs in cells and in the proportion of TIF+ cells at 2 days after DOX treatment (Fig. 3B, 3C). In parallel, we depleted NBS1, which is a component of the MRN complex and is reportedly necessary for the formation of 53BP1-associated TIFs in MEF cells (33), and showed an inhibited TIF formation and reduced proportion of TIF+ cells (Fig. 3B, 3C). In addition, DOX-induced expression of TPP1ΔRD contributed to a greatly exacerbated TIF formation and a higher proportion of TIF+ cells (Fig. 3B, 3C). Collectively, these results demonstrate that histone H3.3 is required for TRF2ΔBΔM-mediated TIF formation and accumulation, and further indicated that H3.3 controls activation of the cGAS-STING pathway by regulating telomeric DDR.

Depletion of H3.3 chaperones inhibits cGAS-STING pathway activation, telomere fusion, and TIF formation

Chaperones of histone H3.3 controls the deposition of histone H3.3 along chromatin DNA (34). Specifically, telomeric histone H3.3 chaperone ATRX-DAXX complex was found to participated in telomere maintenance (35-37). To illustrate that deposition of histone H3.3 on telomeres is important for regulating telomere uncapping-induced IFNβ expression, histone H3.3 chaperone proteins, including anti-silencing function 1 histone chaperone (ASF1), HIRA, ATRX, and DAXX, was depleted by siRNAs in cells expressing TRF2ΔBΔM. Depletion of histone H3.3 chaperones ATRX or DAXX reduced STING phosphorylation and IFNβ expression (Fig. 6A, 6C). Furthermore, depletion of HIRA and ASF1 exerted an obvious inhibitory effect on activation of the cGAS-STING response (Fig. 6B, 6C). Together, these observations indicated that the ATRX, DAXX, HIRA, and ASF1 are all required to activate the cGAS-STING response. To address the participance for these histone chaperone proteins in controlling the telomere uncapping-induced cGAS-STING pathway activation, we further tested the telomeric DDR and telomere fusion in cells with depleted expression of ATRX, DAXX, and HIRA. Depletion of ATRX, DAXX, and HIRA all showed a reduced percentage of fused chromatids and cells with > 5 TIFs (Fig. 6D, S3). The results implicated that the telomere distribution of histone H3.3 is important for telomere uncapping-induced telomeric DDR and fusion, and further suggested that HIRA also participated in loading histone H3.3 on telomeres. Indeed, the H3.3 distribution on telomeres that determined by chromatin immunoprecipitation (ChIP) were reduced in BJ^t cell treated with depleted ATRX, DAXX, or HIRA (Fig. S4). Thus, localization of H3.3 on telomeres is required for the telomere DDR, fusion, and activation of cGAS-STING pathway.

Glioblastoma-linked H3.3 mutants are less efficient at activating the cGAS-STING response

Mutant variants of histone H3.3 have been identified in glioblastomas (38,39). To investigate the effects of such histone H3.3 mutants in terms of how activation of the cGAS-STING response is regulated due to telomere uncapping, constructs expressing histone H3.3 or histone H3.3 mutant variants (i.e., H3.3K27M, H3.3G34R, and H3.3G34V) were transformed into BJ^t cells expressing TRF2ΔBΔM. Ectopic histone H3.3 expression partially rescued activation of the cGAS-STING response in cells in which endogenous histone H3.3 had been depleted (Fig. 2D, S5). Significantly, the histone H3.3 mutant variants exhibited a diminished capability to do so (Fig. S5). These results indicate that the glioblastoma-associated histone H3.3 mutants impair activation of the cGAS-STING response, and further implicate such variants as being loss-of-function histone H3.3 mutants.

Discussion

The exact relationship between telomeres and histone variant H3.3 remains incompletely characterized. Deposition of histone H3.3 on telomeres of mouse ESCs and MEFs was documented (40). A mutational hot spot in a histone H3.3 genes, i.e., *H3F3A*, was found to induce glioblastoma, a type of tumor in which telomere elongation is primarily achieved via the ALT mechanism (38,39). ALT cancers exhibit a telomerase-independent telomere elongation mechanism, displaying characteristics such as formation of ALT-associated PML bodies (APB), reduced ATRX expression, an impaired cGAS-STING pathway, and an activated recombination response for telomere elongation. The actions of glioblastoma-linked histone H3.3 mutants are actively investigated. Recent findings indicate that the histone $H3.3^{K27M}$ variant exert a dominant effect in triggering impaired chromosome segregation, giving rise to micronuclei, aneuploidy, and genetic instabilities (41). In contrast, the histone $H3.3^{G34V}$ variant inhibits expression of the histone demethylase KDM4B, which regulates the formation of ALT features in mouse ESCs (42). Our observations presented herein reveal that histone H3.3 participates in regulating telomere fusion events and TIFs in cells with deprotected telomeres (Fig. 3, 4). Moreover, ALT cancer-linked histone H3.3 mutants contribute to impaired activation of the cGAS-STING response (Fig. S4). Given that the cGAS-STING pathway is impaired in ALT cells, we hypothesized that ALT cancer-linked histone H3.3 mutant variants would prove dysfunctional in regulating the cGAS-STING signaling cascade. Indeed, we found that those mutants do not elicit a cGAS-STING response and, in fact, are implicated in the dysregulation of damage response activation and repair at telomeres. Therefore, we suggest that in ALT cancers, histone H3.3 mutation is involved in preventing DNA damage response activation. Inactivation of the DNA damage response by expressing histone H3.3 mutants creates genetic instability, but still enable error-prone genome doubling and rapid cell cycle progression.

The fusion of chromosome ends has been described as a strategy for cells to escape the impacts of telomere shortening (43,44) and associated responses. However, our study shows that telomere fusion events drive activation of the cGAS-STING response, as evidenced by depletion of the DNA repair machinery proteins LIG4 and XRCC4 impairing cGAS-STING activation (Fig 5). Our results demonstrate that this impaired response contributes to rescuing the senescence caused by deprotected telomeres (Fig. 1). Therefore, telomere fusion may also participate in the telomere-deprotection-driven senescence, which is mediated by the cGAS-STING pathway. Recently, an investigation of antimitotic drugs revealed that activation of a cGAS-STING response can be triggered by chromatin fusion (45). Therefore, we propose that telomere fusion to induce a cGAS-STING response represents a transient yet rapid effect in cells undergoing telomeric stress. This supposition is supported by the elevated expression of IFNβ being reduced by the fourth day following induced expression of TRF2ΔBΔM (Fig. S1). Long-term induced expression of TRF2ΔBΔM activates a feedback signaling mechanism to prevent an excessive cGAS-STING response. We suggest that this feedback signaling is mediated by CDK1-modulated cGAS phosphorylation, which prevents self-DNA sensing by cGAS during mitosis (46). Apart from this feedback loop, transient activation of the cGAS-STING response induced by TRF2ΔBΔM expression is sufficient to inhibit cell growth (Fig. 1). Thus, combined, our observations indicate that telomere or chromatin fusion transiently activates the cGAS-STING signaling response to controls cell growth. However, the detailed mechanism requires further investigation.

Loss of ATRX has been reported to elicit ALT-associated phenotypes (26), including the formation of ALT-associated PML bodies (APB) and C-circles, telomere sister chromatid exchange (TSCE), and recombination-dependent telomeric DNA synthesis. ATRX is also believed to deposit histone H3.3 on telomeres (23). Moreover, mutations of histone H3.3 have been linked to ALT cancers (38,39). Therefore, we hypothesize that the expression and deposition of histone H3.3 on telomeres controls the choice of DNA repair machineries, i.e., either non-homologous end joining (NHEJ) or homologous recombination (HR). It has been documented that histone H3.3 participates downstream of the PARP1-CHD2 machinery and facilitates NHEJ on telomeres (47). ATRX participates in both NHEJ (36), and HR (48). In addition, depletion of the histone chaperone ASF1 drives telomere recombination (49) and another histone H3.3 chaperone, HIRA, elicits ALT phenotypes and homology-directed repair (HDR) (50). In our experiments, depletion of histone H3.3 and these chaperones reduced the levels of telomere-to-telomere fusion (Fig. 6). We also observed that depletion of H3.3 and its chaperones impaired TIF formation (Fig. 3, Fig. S3), as well as impaired cGAS-STING activation (Fig. 6). Taken together, our results support that histone H3.3 and its chaperones facilitate NHEJ on telomeres. This outcome indicates that the ALT-associated mutants of histone H3.3 and its chaperones inhibit the preferred use of NHEJ for DNA repair on telomeres, thereby facilitating recombination and prompting manifestation of ALT-associated phenotypes.

Data availability

The original data and images in this study are available from responding author on reasonable request.

Acknowledgements

We thank the imaging core for the technical support in Institute of Molecular Biology (IMB), Academia Sinica. We also thank Nithila Joseph in out lab and John O'Brien as English editor in IMB for the English editing.

Author contributions

Liuh-Yow Chen conceived the study and obtain preliminary observations. Chiao-Ming Huang performed the following experiments and acquire the data for all of the figures. Chiao-Ming Huang and Liuh-Yow Chen wrote the paper. All authors commented on the paper.

Funding

This work was supported by the yearly program from Institute of Molecular Biology (IMB), Academia Sinica.

Conflict of interest statement

None declared.

References

1. Lundblad, V. and Szostak, J.W. (1989) A mutant with a defect in telomere elongation leads to senescence in yeast. *Cell*, **57**, 633-643.
2. van Steensel, B., Smogorzewska, A. and de Lange, T. (1998) TRF2 protects human telomeres from end-to-end fusions. *Cell*, **92**, 401-413.
3. Karlseder, J., Smogorzewska, A. and de Lange, T. (2002) Senescence induced by altered telomere state, not telomere loss. *Science*, **295**, 2446-2449.
4. Karlseder, J., Broccoli, D., Dai, Y., Hardy, S. and de Lange, T. (1999) p53- and ATM-dependent apoptosis induced by telomeres lacking TRF2. *Science*, **283**, 1321-1325.
5. Xu, Y. and Baltimore, D. (1996) Dual roles of ATM in the cellular response to radiation and in cell growth control. *Genes Dev*, **10**, 2401-2410.
6. Carney, J.P., Maser, R.S., Olivares, H., Davis, E.M., Le Beau, M., Yates, J.R., 3rd, Hays, L., Morgan, W.F. and Petrini, J.H. (1998) The hMre11/hRad50 protein complex and Nijmegen breakage syndrome: linkage of double-strand break repair to the cellular DNA damage response. *Cell*, **93**, 477-486.
7. Usui, T., Ogawa, H. and Petrini, J.H. (2001) A DNA damage response pathway controlled by Tel1 and the Mre11 complex. *Mol Cell*, **7**, 1255-1266.
8. Celli, G.B., Denchi, E.L. and de Lange, T. (2006) Ku70 stimulates fusion of dysfunctional telomeres yet protects chromosome ends from homologous recombination. *Nat Cell Biol*, **8**, 885-890.
9. Smogorzewska, A., Karlseder, J., Holtgreve-Grez, H., Jauch, A. and de Lange, T. (2002) DNA ligase IV-dependent NHEJ of deprotected mammalian telomeres in G1 and G2. *Curr Biol*, **12**, 1635-1644.
10. Abdisalaam, S., Bhattacharya, S., Mukherjee, S., Sinha, D., Srinivasan, K., Zhu, M., Akbay, E.A., Sadek, H.A., Shay, J.W. and Asaithamby, A. (2020) Dysfunctional telomeres trigger cellular senescence mediated by cyclic GMP-AMP synthase. *J Biol Chem*, **295**, 11144-11160.
11. Hopfner, K.P. and Hornung, V. (2020) Molecular mechanisms and cellular functions of cGAS-STING signalling. *Nat Rev Mol Cell Biol*, **21**, 501-521.
12. Stetson, D.B. and Medzhitov, R. (2006) Recognition of cytosolic DNA activates an IRF3-dependent innate immune response. *Immunity*, **24**, 93-103.
13. Maciejowski, J., Li, Y., Bosco, N., Campbell, P.J. and de Lange, T. (2015) Chromothripsis and Kataegis Induced by Telomere Crisis. *Cell*, **163**, 1641-1654.
14. Erdal, E., Haider, S., Rehwinkel, J., Harris, A.L. and McHugh, P.J. (2017) A prosurvival DNA damage-induced cytoplasmic interferon response is mediated by end resection factors and is limited by Trex1. *Genes Dev*, **31**, 353-369.
15. Chen, Y.A., Shen, Y.L., Hsia, H.Y., Tiang, Y.P., Sung, T.L. and Chen, L.Y. (2017) Extrachromosomal telomere repeat DNA is linked to ALT development via cGAS-STING DNA sensing pathway. *Nat Struct Mol Biol*, **24**, 1124-1131.
16. Goldberg, A.D., Banaszynski, L.A., Noh, K.M., Lewis, P.W., Elsaesser, S.J., Stadler, S., Dewell, S., Law, M., Guo, X., Li, X. *et al.* (2010) Distinct factors control histone variant H3.3 localization at specific genomic regions. *Cell*, **140**, 678-691.
17. Armache, A., Yang, S., Martinez de Paz, A., Robbins, L.E., Durmaz, C., Cheong, J.Q., Ravishankar, A., Daman, A.W., Ahimovic, D.J., Klevorn, T. *et al.* (2020) Histone H3.3 phosphorylation amplifies stimulation-induced transcription. *Nature*, **583**, 852-857.

18. Ishiuchi, T., Abe, S., Inoue, K., Yeung, W.K.A., Miki, Y., Ogura, A. and Sasaki, H. (2021) Reprogramming of the histone H3.3 landscape in the early mouse embryo. *Nat Struct Mol Biol*, **28**, 38-49.
19. Huang, X.W., Cheng, X.R., Wang, N., Zhang, Y.W., Liao, C., Jin, L.H. and Lei, L. (2018) Histone variant H3.3 and its functions in reprogramming. *Yi Chuan*, **40**, 186-196.
20. Loppin, B. and Berger, F. (2020) Histone Variants: The Nexus of Developmental Decisions and Epigenetic Memory. *Annu Rev Genet*.
21. Alvarez-Astudillo, F., Garrido, D., Varas-Godoy, M., Gutierrez, J.L., Villanueva, R.A. and Loyola, A. (2021) The histone variant H3.3 regulates the transcription of the hepatitis B virus. *Ann Hepatol*, **21**, 100261.
22. Wong, L.H., Ren, H., Williams, E., McGhie, J., Ahn, S., Sim, M., Tam, A., Earle, E., Anderson, M.A., Mann, J. *et al.* (2009) Histone H3.3 incorporation provides a unique and functionally essential telomeric chromatin in embryonic stem cells. *Genome Res*, **19**, 404-414.
23. Wong, L.H., McGhie, J.D., Sim, M., Anderson, M.A., Ahn, S., Hannan, R.D., George, A.J., Morgan, K.A., Mann, J.R. and Choo, K.H. (2010) ATRX interacts with H3.3 in maintaining telomere structural integrity in pluripotent embryonic stem cells. *Genome Res*, **20**, 351-360.
24. Drane, P., Ouararhni, K., Depaux, A., Shuaib, M. and Hamiche, A. (2010) The death-associated protein DAXX is a novel histone chaperone involved in the replication-independent deposition of H3.3. *Genes Dev*, **24**, 1253-1265.
25. Dyer, M.A., Qadeer, Z.A., Valle-Garcia, D. and Bernstein, E. (2017) ATRX and DAXX: Mechanisms and Mutations. *Cold Spring Harb Perspect Med*, **7**.
26. Brosnan-Cashman, J.A., Yuan, M., Graham, M.K., Rizzo, A.J., Myers, K.M., Davis, C., Zhang, R., Esopi, D.M., Raabe, E.H., Eberhart, C.G. *et al.* (2018) ATRX loss induces multiple hallmarks of the alternative lengthening of telomeres (ALT) phenotype in human glioma cell lines in a cell line-specific manner. *PLoS One*, **13**, e0204159.
27. Haase, S., Garcia-Fabiani, M.B., Carney, S., Altshuler, D., Nunez, F.J., Mendez, F.M., Nunez, F., Lowenstein, P.R. and Castro, M.G. (2018) Mutant ATRX: uncovering a new therapeutic target for glioma. *Expert Opin Ther Targets*, **22**, 599-613.
28. Shi, L., Wen, H. and Shi, X. (2017) The Histone Variant H3.3 in Transcriptional Regulation and Human Disease. *J Mol Biol*, **429**, 1934-1945.
29. Guo, X., Deng, Y., Lin, Y., Cosme-Blanco, W., Chan, S., He, H., Yuan, G., Brown, E.J. and Chang, S. (2007) Dysfunctional telomeres activate an ATM-ATR-dependent DNA damage response to suppress tumorigenesis. *EMBO J*, **26**, 4709-4719.
30. Celli, G.B. and de Lange, T. (2005) DNA processing is not required for ATM-mediated telomere damage response after TRF2 deletion. *Nat Cell Biol*, **7**, 712-718.
31. Pampalona, J., Soler, D., Genesca, A. and Tusell, L. (2010) Telomere dysfunction and chromosome structure modulate the contribution of individual chromosomes in abnormal nuclear morphologies. *Mutat Res*, **683**, 16-22.
32. Takai, H., Smogorzewska, A. and de Lange, T. (2003) DNA damage foci at dysfunctional telomeres. *Curr Biol*, **13**, 1549-1556.
33. Dimitrova, N. and de Lange, T. (2009) Cell cycle-dependent role of MRN at dysfunctional telomeres: ATM signaling-dependent induction of nonhomologous end joining (NHEJ) in G1 and resection-mediated inhibition of NHEJ in G2. *Mol Cell Biol*, **29**, 5552-5563.

34. Grover, P., Asa, J.S. and Campos, E.I. (2018) H3-H4 Histone Chaperone Pathways. *Annu Rev Genet*, **52**, 109-130.
35. Lovejoy, C.A., Takai, K., Huh, M.S., Picketts, D.J. and de Lange, T. (2020) ATRX affects the repair of telomeric DSBs by promoting cohesion and a DAXX-dependent activity. *PLoS Biol*, **18**, e3000594.
36. Koschmann, C., Calinescu, A.A., Nunez, F.J., Mackay, A., Fazal-Salom, J., Thomas, D., Mendez, F., Kamran, N., Dzaman, M., Mulpuri, L. *et al.* (2016) ATRX loss promotes tumor growth and impairs nonhomologous end joining DNA repair in glioma. *Sci Transl Med*, **8**, 328ra328.
37. Li, F., Deng, Z., Zhang, L., Wu, C., Jin, Y., Hwang, I., Vladimirova, O., Xu, L., Yang, L., Lu, B. *et al.* (2019) ATRX loss induces telomere dysfunction and necessitates induction of alternative lengthening of telomeres during human cell immortalization. *EMBO J*, **38**, e96659.
38. Schwartzentruber, J., Korshunov, A., Liu, X.Y., Jones, D.T., Pfaff, E., Jacob, K., Sturm, D., Fontebasso, A.M., Quang, D.A., Tonjes, M. *et al.* (2012) Driver mutations in histone H3.3 and chromatin remodelling genes in paediatric glioblastoma. *Nature*, **482**, 226-231.
39. Sturm, D., Witt, H., Hovestadt, V., Khuong-Quang, D.A., Jones, D.T., Konermann, C., Pfaff, E., Tonjes, M., Sill, M., Bender, S. *et al.* (2012) Hotspot mutations in H3F3A and IDH1 define distinct epigenetic and biological subgroups of glioblastoma. *Cancer Cell*, **22**, 425-437.
40. Szenker, E., Ray-Gallet, D. and Almouzni, G. (2011) The double face of the histone variant H3.3. *Cell Res*, **21**, 421-434.
41. Bockaj, I., Martini, T.E.I., de Camargo Magalhaes, E.S., Bakker, P.L., Meeuwsen-de Boer, T.G.J., Armandari, I., Meuleman, S.L., Mondria, M.T., Stok, C., Kok, Y.P. *et al.* (2021) The H3.3K27M oncohistone affects replication stress outcome and provokes genomic instability in pediatric glioma. *PLoS Genet*, **17**, e1009868.
42. Udugama, M., Hii, L., Garvie, A., Cervini, M., Vinod, B., Chan, F.L., Das, P.P., Mann, J.R., Collas, P., Voon, H.P.J. *et al.* (2021) Mutations inhibiting KDM4B drive ALT activation in ATRX-mutated glioblastomas. *Nat Commun*, **12**, 2584.
43. Cleal, K., Norris, K. and Baird, D. (2018) Telomere Length Dynamics and the Evolution of Cancer Genome Architecture. *Int J Mol Sci*, **19**.
44. Capper, R., Britt-Compton, B., Tankimanova, M., Rowson, J., Letsolo, B., Man, S., Haughton, M. and Baird, D.M. (2007) The nature of telomere fusion and a definition of the critical telomere length in human cells. *Genes Dev*, **21**, 2495-2508.
45. Flynn, P.J., Koch, P.D. and Mitchison, T.J. (2021) Chromatin bridges, not micronuclei, activate cGAS after drug-induced mitotic errors in human cells. *Proc Natl Acad Sci U S A*, **118**.
46. Zhong, L., Hu, M.M., Bian, L.J., Liu, Y., Chen, Q. and Shu, H.B. (2020) Phosphorylation of cGAS by CDK1 impairs self-DNA sensing in mitosis. *Cell Discov*, **6**, 26.
47. Luijsterburg, M.S., de Krijger, I., Wiegant, W.W., Shah, R.G., Smeenk, G., de Groot, A.J.L., Pines, A., Vertegaal, A.C.O., Jacobs, J.J.L., Shah, G.M. *et al.* (2016) PARP1 Links CHD2-Mediated Chromatin Expansion and H3.3 Deposition to DNA Repair by Non-homologous End-Joining. *Mol Cell*, **61**, 547-562.
48. Elbakry, A., Juhasz, S., Chan, K.C. and Lobrich, M. (2021) ATRX and RECQ5 define distinct homologous recombination subpathways. *Proc Natl Acad Sci U S A*, **118**.

49. O'Sullivan, R.J., Arnoult, N., Lackner, D.H., Oganesian, L., Haggblom, C., Corpet, A., Almouzni, G. and Karlseder, J. (2014) Rapid induction of alternative lengthening of telomeres by depletion of the histone chaperone ASF1. *Nat Struct Mol Biol*, **21**, 167-174.
50. Hoang, S.M., Kaminski, N., Bhargava, R., Barroso-Gonzalez, J., Lynskey, M.L., Garcia-Exposito, L., Roncaioli, J.L., Wondisford, A.R., Wallace, C.T., Watkins, S.C. *et al.* (2020) Regulation of ALT-associated homology-directed repair by polyADP-ribosylation. *Nat Struct Mol Biol*, **27**, 1152-1164.

Figures

Figure 1.

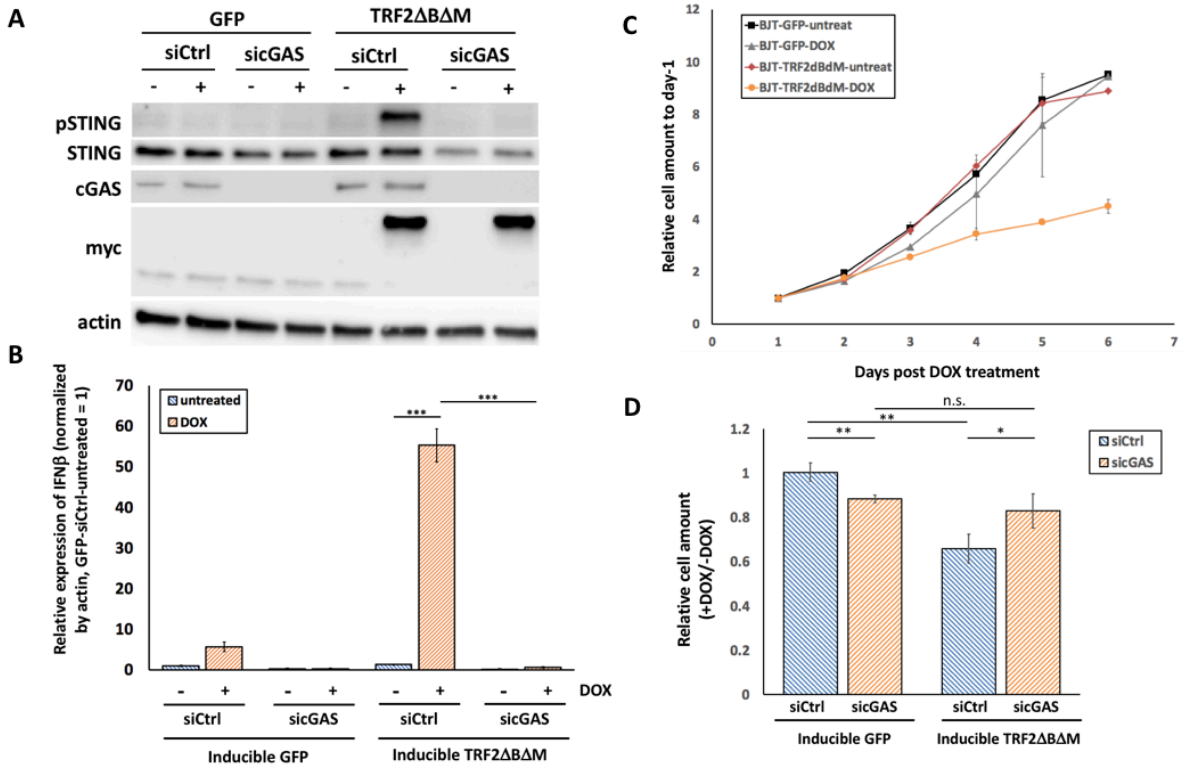

Expression of TRF2ΔBΔM triggers cGAS-STING pathway activation and cGAS-mediated growth inhibition. BJ^t cells were separated into untreated and treatment groups, and 25 ng/ml doxycycline (DOX) was mixed into the culture medium of the treatment group to induce expression of TRF2ΔBΔM. siRNAs were added twice, i.e., at 60 h and 12 h before inducing expression via 2.5 ng/ml doxycycline (DOX). (**A**) Protein levels of phosphorylated STING S366 (pSTING), STING, cGAS, myc, and actin were determined by Western blotting. (**B**) The expression level of IFNβ mRNA was determined by RT-qPCR. qPCR experiments represent the mean ±SD of three technical repeats. (**C**) Numbers of surviving cells under the indicated conditions were determined by counting the DAPI signals in the culture dishes. Number of cells was normalized to day-1 after treatment in each experiment. Data represent the mean ±SD of three biological repeats. (**D**) Two sets of BJ^t cells—inducibly expressing GFP or TRF2ΔBΔM—were treated with or without 25 ng/ml DOX. Surviving cells were counted 4 days after later.

Figure 2.

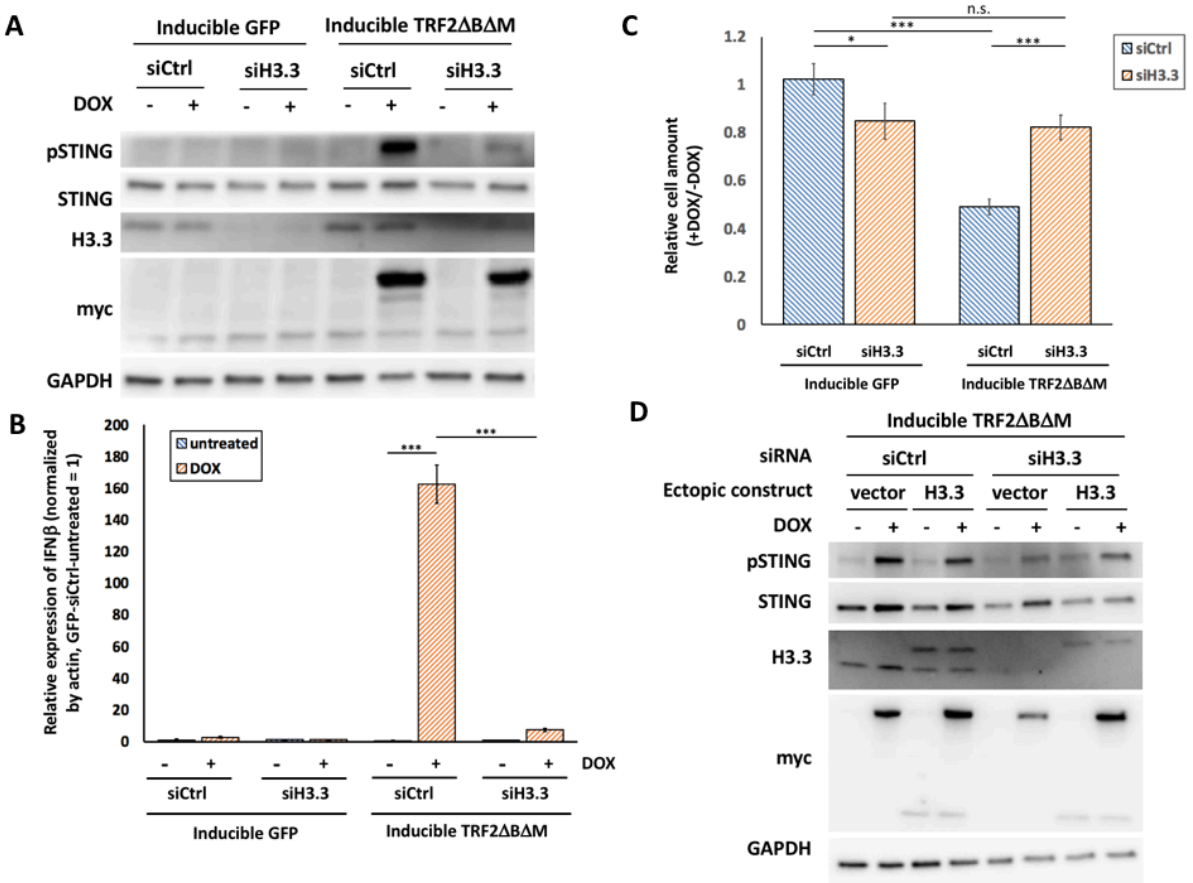

Depletion of H3.3 impairs cGAS-STING pathway activation and rescues growth defects due to expression of TRF2ΔBΔM. (**A**) BJ^t cells stably expressing GFP or myc-tagged TRF2ΔBΔM were established. siRNAs were added twice, i.e., at 60 h and 12 h before inducing expression with doxycycline (DOX). Samples were cultured for 2.5 days to investigate the cGAS-STING signaling response. Protein levels of phosphorylated STING (pSTING), STING, H3.3, myc, and GAPDH were determined by Western blotting. (**B**) mRNA expression levels of IFNβ were determined by RT-qPCR. qPCR experiments represent the mean ±SD of three technical repeats. (**C**) Numbers of cells in the DOX+ or DOX- treatment groups were counted to evaluate cell growth 4 days later. Data represent the mean ±SD of three biological repeats. (**D**) A siRNA-insensitive H3.3 construct was introduced into cells via viral vectors and ectopically expressed. Protein levels of phosphorylated STING (pSTING), STING, H3.3, myc, and GAPDH were then determined by Western blotting.

Figure 3.

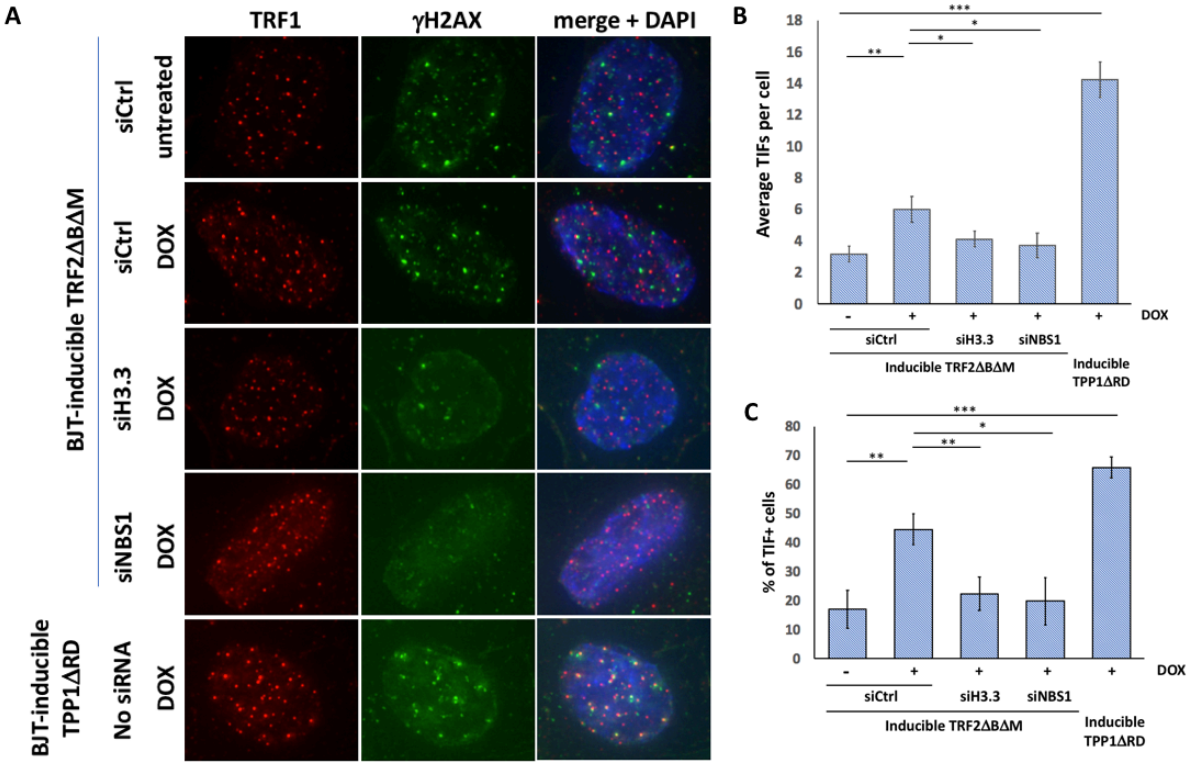

Depletion of H3.3 expression limits TIF formation. BJ^t cells were treated with siRNAs including siCtrl, siH3.3, siNBS1 at 60 h and 12 h before the inducing stable expression of TRF2ΔBΔM or TPP1ΔRD by means of 2.5 ng/ml DOX treatment. (**A**) Immunostaining of γH2AX and TRF1 was performed on day 2 after DOX treatment. Representative images stained for γH2AX (green) and TRF1 (red). (**B**) Average numbers of TIFs per cell in the different treatment groups. (**C**) Percentages of cells harboring >5 TIFs. For each sample in each repeat, more than 100 cells were quantified. Data represent mean ±SD of three biological repeats.

Figure 4.

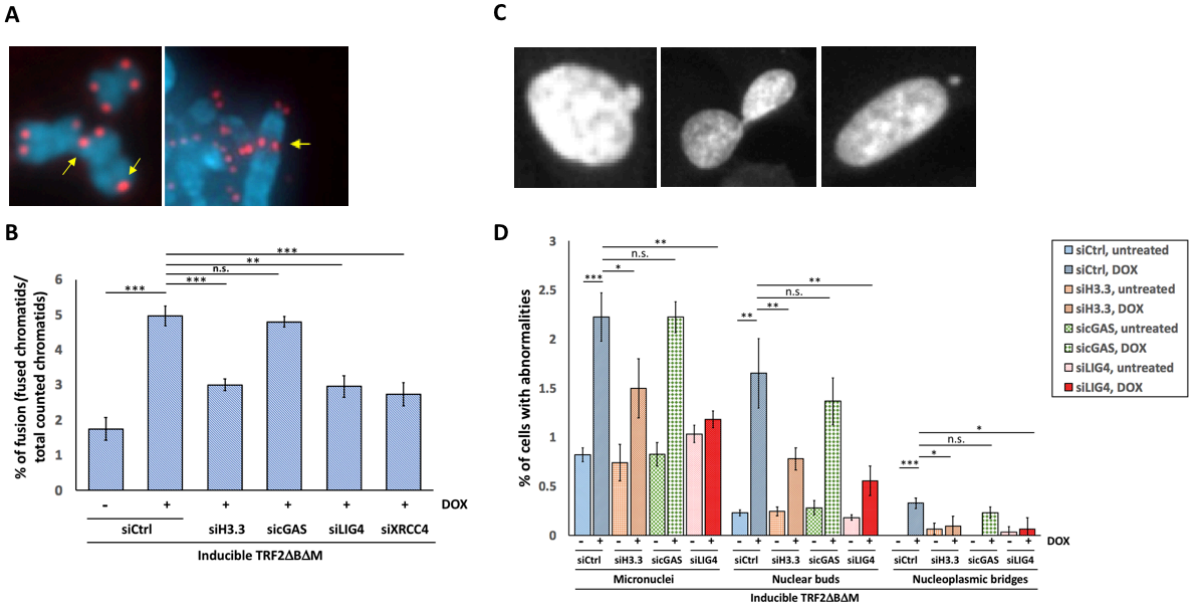

Depletion of H3.3 expression limits telomere-to-telomere fusion events and the formation of nuclear abnormalities. BJ^t cells were treated with siRNAs including siCtrl, siH3.3, sicGAS, siLIG4, and siXRCC4 at 60 h and 12 h before DOX treatment to induce expression of TRF2ΔBΔM for 24 h. Cells were arrested using 0.1 μg/ml Demecolcine for another 24 h, and then spread on a slide to visualize telomere-to-telomere fusion events by staining with a TelC probe. (**A**) Representative images of telomere-to-telomere fusion events (yellow arrows). (**B**) Quantitative results for telomere-to-telomere fusion events calculated from >2000 chromosomes for each sample. Data represent mean ±SD of three biological repeats. (**C**) Representative cells images of siRNA-treated cells on day 2 after DOX treatment. For each group, >1,000 nuclear images were acquired and counted to determine percentages of the indicated nuclear abnormalities. Representative images are shown for a nuclear bud (left), a nucleoplasmic bridge (middle), a micronucleus (right) are given. (**D**) Quantitative results for nuclear abnormalities. Data represent the mean ±SD of three technical repeats.

Figure 5.

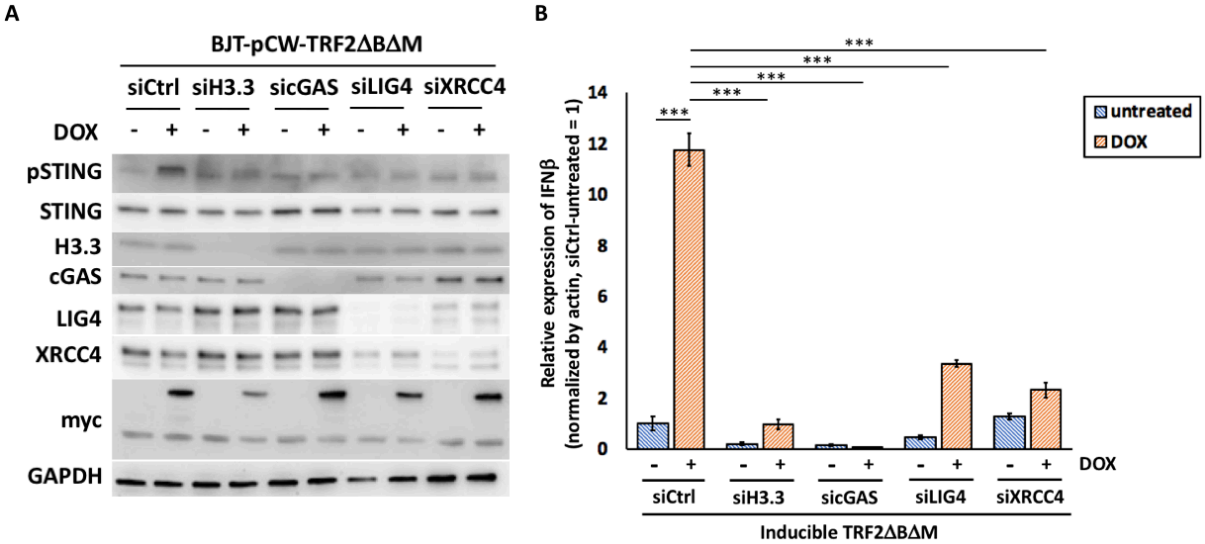

Depletion of LIG4 and XRCC4 disrupts the activation of the cGAS-STING response. BJ^t cells inducibly expressing myc-tagged TRF2ΔBΔM were treated with siRNAs at 60 h, and 12 h before doxycycline (DOX) treatment. To correlate telomere fusion events and nuclear abnormalities, treated cell were lysed on day 2 after DOX treatment. (**A**) Protein levels of phosphorylated STING (pSTING), STING, H3.3, cGAS, LIG4, XRCC4, myc, and GAPDH were determined by Western blotting. (**B**) mRNA expression levels of IFNβ were determined by RT-qPCR. qPCR experiments represent the mean ±SD of three technical repeats.

Figure 6.

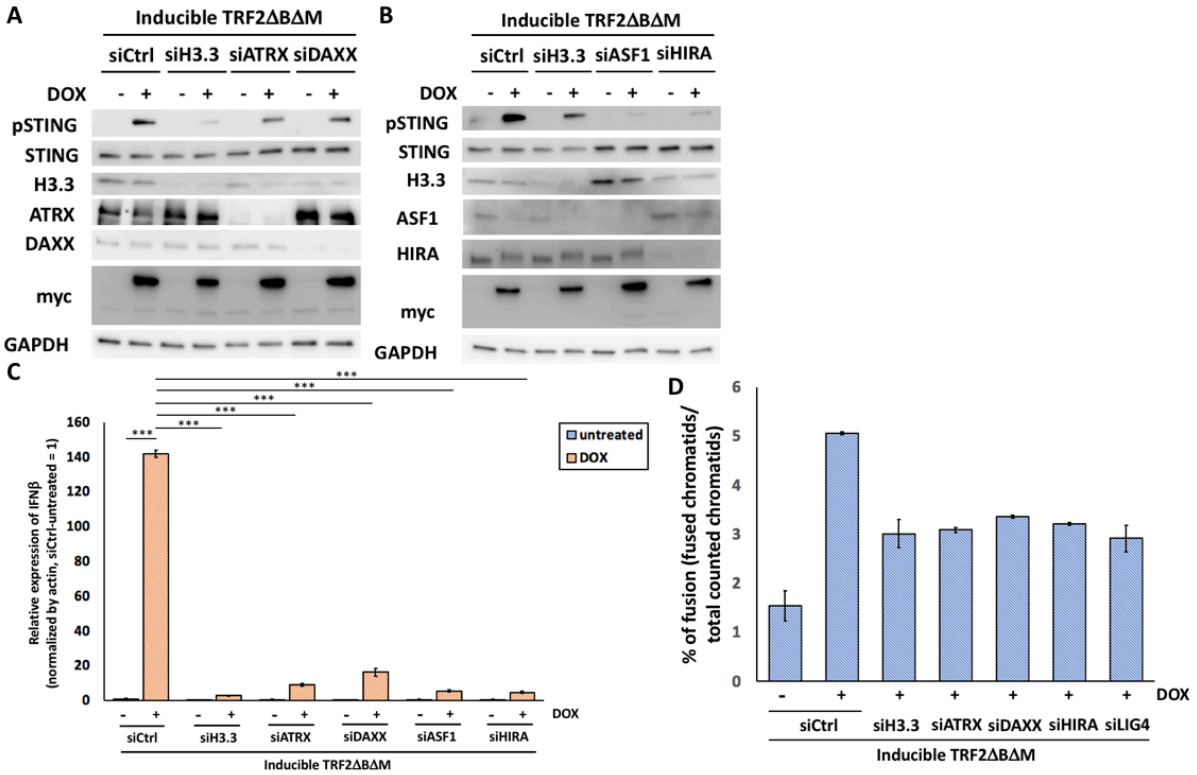

Depletion of H3.3 chaperones impairs cGAS-STING pathway activation. BJ^t cells were treated with siRNAs at 60 h and 12 h before inducing expression of myc-tagged TRF2ΔBΔM with doxycycline (DOX). Samples were cultured for 2.5 days to investigate the cGAS-STING signaling response. (**A**, **B**) Protein levels of phosphorylated STING (pSTING), STING, ASF1, HIRA, ATRX, DAXX, H3.3, myc, and GAPDH were determined by Western blotting. (**C**) mRNA expression levels of IFNβ were determined by RT-qPCR. qPCR experiments represent the mean ±SD of three technical repeats. Another set of BJ^t cells were treated with siRNAs including siCtrl, siH3.3, siATRX, siDAXX, siHIRA, and siLIG4 at 60 h and 12 h before DOX treatment to induce expression of TRF2ΔBΔM for 24 h. Cells were arrested using 0.1 μg/ml Demecolcine for another 24 h, and then spread on a slide to visualize telomere-to-telomere fusion events by staining with a TelC probe. (**D**) Quantitative results for telomere-to-telomere fusion events calculated from >2000 chromosomes for each sample. Data represent the mean ±SD of two set of experiments.